IEEE TRANSACTIONS ON
CIRCUITS AND SYSTEMS
I: REGULAR PAPERS

IEEE Xplore® Digital Library
http://ieeexplore.ieee.org/Xplore

Design of Synthetic Central Pattern Generators Producing Desired Quadruped Gaits

Matteo Lodi, Andrey Shilnikov, Marco Storace, *Senior Member, IEEE*

Abstract—**This paper is concerned with a method for design and analysis of specific neuronal networks, called central pattern generators (CPGs), which produce primary rhythmic patterns in animals. In particular, the paper is focused on synthetic CPGs made up of few basic elements and governing quadrupeds' gaits and gait transitions, under the control of an external drive. The method combines principles of bifurcation theory, geometric properties of symmetry, and numerical analysis based on the recently proposed toolbox CEPAGE. The method is applied to two CPGs, one bio-inspired and one purely synthetic. In both cases, the method provides a way to obtain a desired sequence of gaits by continuously changing a bifurcation parameter related to the external drive.**

Index Terms—**Central pattern generators, dynamical systems, bifurcation analysis.**

I. Introduction

The motor circuits in the spinal cord that control locomotion are commonly referred to as *central pattern generators* (CPGs). A CPG is a neuronal network that is capable of generating an organized pattern of motor activity independently of sensory inputs, thus producing primary rhythmic behaviors such as respiration, mastication, sucking, crawling, flying, swimming and walking [1]. In vertebrates, the planning of muscle activity involves many supra-spinal networks, which activate the CPGs that determine the gaits [2]–[7]. The CPG functions include selecting which muscles are to be activated, how intensely and for how long, thus allowing patterns of movements of widely varying strengths and speeds, whereas the supra-spinal networks drive the outputs from the CPG (allowing gait changes and adaptation to obstacles and uncertainties during ambulatory excursions [8]) on the basis of both sensory feedback pathways and vestibular pathways [9]–[11]. This combination of closed-loop and open-loop control systems allows obtaining a robust control of locomotion, characterized by rhythmicity (the specific periodic pattern provided by the CPG), stability against perturbations and noise (the pattern corresponds to self-sustained oscillation due to a stable limit cycle), adaptability (owing to the feedback pathways), and variety (by changing the gaits) [12]–[16].

One of the fundamental challenges in motor systems neuroscience is discovering the intrinsic functional mechanisms of CPG networks and the way in which they integrate descending inputs from the brain-stem, which are in turn under the control of basal ganglia and cortex [3], [17]. This challenge is faced both by biology and related disciplines – whose main aim is fully understanding the CPG physiological structure and functionality – and by nonlinear dynamics, whose main aims are understanding the functionality of the underlying mechanisms and modeling with the simplest dynamical networks either a real structure (bio-inspired CPG) or just specific functionalities (synthetic CPG), either by resorting to group theory [18] or to multi-parameter bifurcation theory [19]–[21]. Moreover, the main aim of engineering is designing and implementing CPGs on embedded circuits for specific applications [12], [22], mainly in the fields of bio-robotics [23], [24] and rehabilitation [25], [26].

Then, the acronym CPG is used to denote both the real neuronal network (which in vertebrates can be composed of hundreds/thousands of neurons) and its model. Since in the real network there are groups of neurons that behave coherently and whose concerted activity can be modeled as a unique functional module (called in many ways, e.g., *cell*, *unit*, *oscillator*, *neuron*), the CPG intended as model is always composed of few cells. The complete CPG function is the result of neural circuits containing these modules as elementary blocks. Henceforth, unless otherwise stated, CPG will denote a model of a real neuronal network.

In this paper we propose a method for designing and analyzing CPGs, based on multi-parameter bifurcation theory. Of course, the method is independent of the tools used to implement it, but here we will use a recently proposed software tool (called CEPAGE) [27].

The proposed strategy is illustrated through two case studies, related to locomotion and gait transitions in quadrupeds, which are in turn novelty elements of this paper. The first case study is an 8-cell bio-inspired CPG controlling gaits in quadrupeds [28]. Despite the complexity of both the real CPG and its 40-cell model described in [28], the proposed 8-cell CPG model is able to capture the main functional behaviors of the real CPG. This has a twofold advantage: firstly, the simplification points out the role played by the main components of the network; secondly, the reduced network has a lower computational complexity and then it can be exploited to improve simulation speed or to implement an embedded system able to mimic the network behavior in a real-time environment.

The second case study is a 4-cell purely synthetic CPG, which is designed to obtain the same gait transitions as before. In both cases, by following some prescribed steps, we obtain

M. Lodi and M. Storace are with the Department of Electrical, Electronic, Telecommunications Engineering and Naval Architecture, University of Genoa, Via Opera Pia 11a, I-16145, Genova, Italy. A. Shilnikov is with the Neuroscience Institute, Georgia State University, 100 Piedmont Ave, Atlanta GA 30303, USA. E-mail: marco.storace@unige.it. This work was partially supported by the University of Genoa, by NSF BIO-DMS (grant IOS-1455527), and by Lobachevsky University of Nizhny Novgorod (RSF grant 14-41-000440).

Digital Object Identifier: 10.1109/TCSI.2017.2759320

1558-0806 © 2017 IEEE. Personal use is permitted, but republication/redistribution requires IEEE permission.
See http://www.ieee.org/publications_standards/publications/rights/index.html for more information.

the desired gait transitions by acting on a bifurcation parameter modeling the supra-spinal networks driving.

This paper is structured as follows. Section II briefly describes the working framework, i.e., how a CPG can be modeled and the main features of CEPAGE. The proposed design and analysis strategy is described in Sec. III, whereas the two case studies are analyzed in Secs. IV and V. Finally, some conclusions are drawn in Sec. VI.

II. CPGs and CEPAGE

In this section we briefly describe the building elements of a CPG model, the phase-difference representation used in CEPAGE to analyze them, and the main toolbox features.

A. CPG models

A CPG model is basically defined by two elements:

- the cell, which can be a neuron model (e.g., Hodgkin-Huxley, FitzHugh-Nagumo, Morris-Lecar, Hindmarsh-Rose, integrate-and-fire models) or another oscillator (e.g., Kuramoto, Hopf, Van der Pol);
- the connections (synapses) between cells, which define the CPG topology and can be electrical, chemical inhibitory or chemical excitatory.

A third possible element (CPG input, when it does not work autonomously) is the brain-stem drive, which brings an input to the CPG from supra-spinal networks, allowing gait changes and adaptation.

CEPAGE models a CPG composed of N cells, each described by the following dynamical system ($i = 1, \ldots, N$):

$$\dot{\mathbf{z}}_i = \begin{bmatrix} \dot{V}_i \\ \dot{\mathbf{x}}_i \end{bmatrix} = \begin{bmatrix} f_i(\mathbf{z}_i, \alpha, I_{syn}^{(i)}(\alpha)) \\ \mathbf{p}_i(\mathbf{z}_i) \end{bmatrix} \tag{1}$$

Assuming that the cell is a neuron model, V_i is the membrane voltage, $\mathbf{x}_i$ is a vector containing the other state variables (whose dynamics are described by the vector field $\mathbf{p}_i$), α is a parameter related to the brain-stem drive, and $I_{syn}^{(i)}(\alpha)$ is the incoming synaptic current, containing the following contributions:

$$\begin{aligned} I_{syn}^{(i)} = & \sum_{j=0}^{N-1} g_{ij}^{in}(\alpha) h_{in}(V_i, V_j, \mathbf{s}_{ij}^{in}) + \\ & \sum_{j=0}^{N-1} g_{ij}^{ex}(\alpha) h_{ex}(V_i, V_j, \mathbf{s}_{ij}^{ex}) + \sum_{j=0}^{N-1} g_{ij}^{el}(\alpha)(V_j - V_i) \end{aligned} \tag{2}$$

where h_{in} and h_{ex} describe generic chemical inhibitory and chemical excitatory synapses actions, respectively, and in general depend on the pre-synaptic and post-synaptic cell membrane potentials (V_j and V_i, respectively) and on the state $\mathbf{s}_{ij}^{xx}$ of the synapse of type xx between cells i and j, which evolves according to a nonlinear dynamical system $\dot{\mathbf{s}}_{ij}^{xx} = \hat{\mathbf{f}}(\mathbf{s}_{ij}^{xx}, V_j)$. The functions $g_{ij}^{in}(\alpha)$, $g_{ij}^{ex}(\alpha)$ and $g_{ij}^{el}(\alpha)$ represent chemical inhibitory, chemical excitatory and electrical synapses strengths, respectively, between cells i and j and in general depend on the brain-stem drive through the parameter α. If a synaptic strength does not depend on α, it reduces to a constant coefficient; $g_{ij}^{xx} = 0$ means that cells i and j are not connected by synapses of type xx. In this paper, the synaptic actions have no dynamics and are modeled according to the fast threshold modulation paradigm [29], as follows:

$$\begin{aligned} h_{in}(V_i, V_j) &= \frac{E_{in} - V_i}{1 + e^{\nu(V_j - \theta)}}, \\ h_{ex}(V_i, V_j) &= \frac{E_{ex} - V_i}{1 + e^{\nu(V_j - \theta)}}, \end{aligned} \tag{3}$$

where E_{in} and E_{ex} are the inhibitory and excitatory synapses reverse potentials, respectively, whereas ν and θ act on the chemical synapses activation function shape.

B. Analysis strategy

In this paper the CPG are analyzed following the so-called phase-lag or phase-difference representation of oscillatory or bursting cells coupled in a network [13], [14], [16], [30], [31], which allows checking the existence and stability of rhythmic patterns generated by the network by using standard tools of nonlinear dynamics. A first assumption underlying this method is that all cells remain oscillatory with relatively close temporal characteristics. This means that each i-th cell stays on a structurally stable periodic orbit $\hat{\mathbf{z}}_i(t)$ of period T_i and that this orbit can be mapped (through the modulo function) to a phase variable $\phi_i \in [0, 1)$ so that ϕ_i is reset to 0 when V_i grows over a threshold V_{th}.

The phase difference representation of the network employs $N - 1$ state variables describing phase differences between the reference cell 1 and the other network cells: $\Delta\phi_{1i}(t) = (\phi_i(t) - \phi_1(t)) \mod 1$ ($i = 2, \ldots, N$). The time evolution of these state variables is unknown *a priori* and is usually determined numerically by integrating multiple initial conditions of (1) to reveal possible multi-stability.

From a numerical standpoint, the phase differences can be computed as follows. Let $t_i(k)$ be the k-th time at which the membrane voltage V_i of the i-th cell overcomes the threshold V_{th}. The phase lag $\Delta\phi_{1i}(k)$ between the i-th cell and the reference cell 1 can be numerically computed as follows:

$$\Delta\phi_{1i}(k) = \frac{t_i(k) - t_1(k)}{T_1} \mod 1, \tag{4}$$

where T_1 is the period of the first cell. As the time progresses these phase lags can converge and stabilize at some stable phase-locked states, possibly more than one (multi-stability of the network).

This representation is adopted also in Motiftoolbox [32].

C. Toolbox features

CEPAGE is an object-oriented toolbox for simulation and analysis of CPGs [27]. It has a two-layer organisation: the outer layer is a MATLAB interface that makes it easy to specify the CPG configuration and offers tools for data analysis and visualization; the inner layer is used for numerical integrations

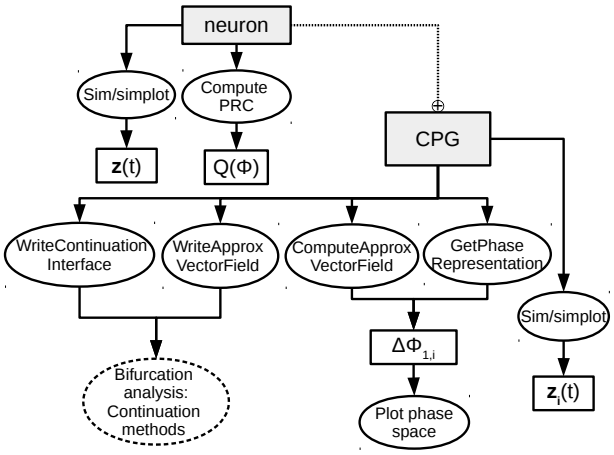

Fig. 1. Relationships between CEPAGE objects.

and is based on Boost C++ libraries and on MEX files.[1] The MATLAB layer provides flexibility to CEPAGE, since it makes it easy to add new neuron and synapse models to be simulated and new functionalities to the package by extending the base classes. Moreover, MATLAB allows the user to write very concise and clear scripts, which nonetheless retain the full power and speed of the underlying C/C++ code.

Figure 1 shows the functional relationships between classes (gray boxes), main methods (solid ellipses) and corresponding output data (white boxes). The dashed ellipses denote external analysis tools that can be applied to the obtained data. Parallel computation, MEX files and the Boost C++ libraries are used to reduce the simulation times. The classes *neuron*, *synapse* and *CPG* describe a single cell, a synapse and a CPG, respectively.

The main toolbox functionalities are:

-) simulation of CPGs: by using method *sim* of class *CPG*, the user can easily obtain the time evolution of the state variables describing the network; it is also possible to start parallel simulations from different initial conditions. If only one initial condition is considered, it is possible to use the *simplot* method, which also plots the state evolution;

-) limit cycle continuation; this functionality is useful when one wants to detect limit cycle bifurcations; through the method *writeContinuationInterface*, it is possible to generate AUTO [33] or MATCONT [34] files for the limit cycle continuation;

-) CPG phase difference simulation: the method *getPhaseRepresentation* of class *CPG* allows obtaining the evolution of the phase differences for the CPG cells; also in this case, parallel computations can be exploited to integrate the system starting from different initial conditions. The simulation results can then be plotted through the *plotPhaseSpace* method. This functionality can be used to obtain a brute-force bifurcation diagram of the phase differences, but turns out to be very time consuming for relatively large networks;

-) CPG approximate phase difference simulation: the method *computeApproxVectorField* of class *CPG* is useful to carry out brute-force (i.e., based on numerical integrations and Poincaré sections [35]) analysis of the phase differences between cells reducing the simulation times. The approximate solution works accurately only for weakly-coupled networks and is computed starting from the so-called Phase Resetting Curve (PRC) [36], which can be computed through the method *computePRC* of class *neuron model*;

-) phase difference continuation: the approximate formulation allows also knowing the vector field that describes the phase difference evolution, making it possible a continuation analysis of the patterns generated by the network. CEPAGE can automatically generate files through the method *writeApproxVectorField*, which can be used to carry out continuation analysis with AUTO or MATCONT.

[1]A MEX file is a type of computer file that provides an interface between MATLAB and functions written in C, C++ or Fortran. It stands for "MATLAB executable". When compiled, MEX files are dynamically loaded and allow external functions to be invoked from within MATLAB as if they were built-in functions.

TABLE I
GAIT CHARACTERISTICS IN TERMS OF DUTY-CYCLE (**dc**) AND PHASE DIFFERENCES BETWEEN LEGS (L=LEFT, R=RIGHT, F=FORE, H=HIND).

Gait	**dc**	$\Delta\varphi_{RF-LF}$	$\Delta\varphi_{RF-LH}$	$\Delta\varphi_{RF-RH}$
Walk	**0.25**	**0.5**	**0.75**	**0.25**
Trot	**0.5**	**0.5**	**0**	**0.5**
Bound	**0.65**	**0**	**0.5**	**0.5**
Transverse gallop	**0.6**	**0.1(0.9)**	**0.7(0.5)**	**0.6**
Rotary gallop	**0.6**	**0.1(0.9)**	**0.4(0.7)**	**0.6**

III. SYNTHETIC CPG DESIGN METHOD

CEPAGE can be used as a tool to design a synthetic CPG able to generate some specific gaits typical of quadrupeds (i.e., trot, walk, bound, rotary gallop, transverse gallop) either by varying a bifurcation parameter in an assigned (e.g., bio-inspired) CPG with fixed structure or by designing (including the structure) a purely synthetic CPG. In both cases, our goal is finding – for the cells or synapses directly depending on the brain-stem drive through the parameter α – proper functions of α that allow obtaining the desired gaits and gait transitions. To this end, according to the framework described in Sec. II-A, we introduce an explicit dependence on α of some parameters and we choose piecewise-linear (PWL) functions, connecting points detected through bifurcation analysis.

Table I shows the main characteristics of each gait we want to achieve. The duty cycle properties of each gait are common for many quadrupeds, whereas gait amplitude and frequency depend on each specific animal. In this work (case study 1), we focus on the amplitude and frequency values typical for a mouse [28]. A representation of the different gaits is provided as supplemental material.

We assume that each limb is driven by a cell, then we will consider CPGs containing at least four cells. The proposed strategy can be used for any gait with left-right symmetry. It can be applied also to asymmetric gaits (possibly with few changes, as shown in Sec. V-E).

The proposed design steps to obtain a specific symmetric gait are as follows:

- **Step 1**: we analyze a simple structure (which appears more than once in an assigned CPG or is used as building

block in a purely synthetic CPG), typically an half-center oscillator (HCO). By carrying out a bifurcation analysis, we can analyze the possible stable behaviors of this structure with respect to the chosen bifurcation parameter. The desired behaviors correspond to a specific range of values of this parameter. Finally, we relate this range to the external drive α through a PWL function.

- **Step 2**: we analyze the CPG sub-structure (either the simple structure of Step 1 or a more complex subset of CPG elements) which governs left-right (LR) coordination; this sub-structure usually contains both inhibitory and excitatory synapses. By choosing the strength of the excitatory synapses as a proper PWL function of α, we can vary the phase difference between the patterns generated by each cell of the sub-structure. CEPAGE is used to obtain bifurcation diagrams that serve as design maps.
- **Step 3**: we analyze the behavior of the complete CPG (or of a part of it, in the presence of symmetries) by analyzing the influence of α on the fore-hind (FH) coordination. Even when changing α, we must ensure the structural stability of both LR and FH coordinations. By choosing proper parameter settings (selected through a bifurcation analysis carried out with CEPAGE), the CPG can generate robust patterns. By making some parameters become proper PWL functions of α connecting the robust patterns, we can also obtain a desired sequence of gait transitions.
- **Step 4**: *a posteriori* analysis of the complete CPG, if not already carried out in Step 3.

In the next sections, two examples of application of this strategy will be proposed: the first case study is concerned with the analysis of a bio-inspired 8-cell CPG with assigned structure and with the design of a synthetic CPG with the same (fixed) structure; the second case study is the design of a purely synthetic 4-cell CPG. In both cases, the main aim is to generate the cited gaits typical of quadrupeds.

IV. Case study 1: bio-inspired CPG

In this section we will show how CEPAGE can be used to analyze a 8-cell CPG and to set its parameters in order to generate all the gaits listed in Table I.

In particular, in [28] a quadrupedal 40-cell CPG is described and analyzed, which is able to generate trot, walk and bound. The brain-stem drive acts directly on some CPG cells through the parameter α, ranging in the interval $[0, 1]$.

With respect to the 40-cell CPG, the proposed 8-cell CPG (shown in Fig. 2) maintains only the neuron populations directly driving flexor (central cells, from 1 to 4, where L=left, R=right, F=fore, H=hind) and extensor (cells from 5 to 8) muscles in each leg. The other populations are replaced by fast chemical synapses, inhibitory (ending with a filled circle) or excitatory (ending with a filled square), depending on the nature of the replaced population, thus obtaining the 8-cell CPG. Indeed, the removed populations basically behave as amplifiers, without introducing significant delays in the action potential transmission to flexors and extensors [37], [38].

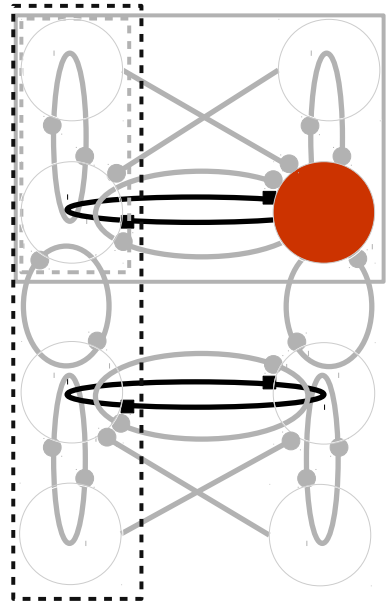

Fig. 2. (Color online) Structure of the 8-cell CPG. The central cells (1–4) drive flexor muscles in each leg (L=left, R=right, F=fore, H=hind), whereas upper and lower cells (5–8) drive the corresponding extensor muscles. (Chemical) synapses, either inhibitory (ending with filled circles) or excitatory (ending with filled squares), are represented by gray connections. The excitatory connections depending on the brain-stem drive are shown in black.

Since in the 40-cell CPG the brain-stem drive acts on excitatory neuron populations here replaced by excitatory synapses, we model this effect by introducing a nonlinear and monotonically increasing dependence of the corresponding synaptic efficacies g_{ij}^{ex} on the parameter α, according to Eq. (2). This accounts for another key feature of CPGs, i.e., the differential recruitment of cells during various motor behaviors. In particular, some cells are active during different types of movement, whereas other cells are selectively recruited for each task [1], [39]–[42].

The functions $g_{ij}^{ex}(\alpha)$ have been identified through a polynomial fitting, such that the 8-cell network behaves as the 40-cell CPG with respect to $\Delta\phi_{12}$. The fitting provided 10-th order polynomials (see Appendix A).

The other synaptic efficacies are assumed to be constant (the non-zero values are listed in Tab. II in Appendix A). Their values have been determined by optimization, in order to reproduce the behavior of the original 40-cell CPG.

Each cell is modeled in CEPAGE through the same neuron model used in [28] (see Appendix A), for the sake of comparison, where the parameters have the same values as in [28] and are reported in Appendix A.

About the synapses, here (unlike in [28]) we use the more biophysically plausible model (2).

A. Analysis

We analyzed the CPG behavior by varying the bifurcation parameter α, as in [28].

Each flexor cell eventually produces the same periodic spiking pattern, but with different phase. Figure 3 shows the spiking frequency f (upper panel) and duty cycle dc vs. α for

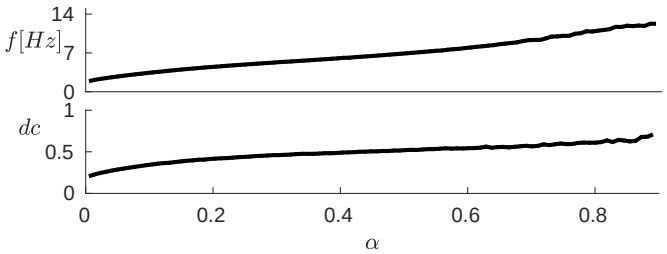

Fig. 3. Spiking frequency **f** (upper panel) and duty cycle **dc** of each flexor cell vs. **α**.

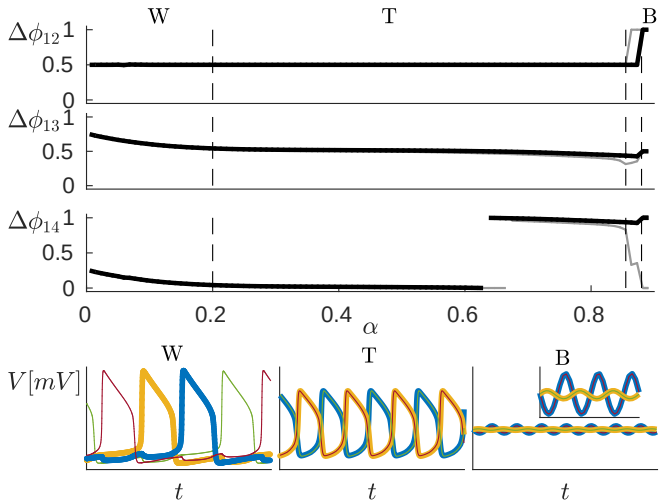

Fig. 4. (Color online) Upper panels: 1D bifurcation diagrams $\Delta\varphi_{1i}(\alpha)$, with $i = 2$ (top panel), $i = 3$ (middle panel), $i = 4$ (bottom panel), obtained by increasing (black lines) or decreasing (gray lines) the bifurcation parameter α. The bifurcation diagrams point out the regions where walk (W), trot (T) and bound (B) are the only stable gait. Bottom panels: membrane voltages $V_i(t)$ (ranging in the interval $[-60, -10]$mV) for the flexor cells in the three regions W (left panel), T (central panel) and B (right panel), over a window of 600ms (the color code is the same as for the cells in Fig. 2).

each flexor cell. It is evident that both f and dc increase with α and this is perfectly coherent with the results reported in [28].

The stable phase differences $\Delta\phi_{1j}$ ($j = 2, 3, 4$) vs. α are shown in the three upper panels of Fig. 4. By varying α, the CPG is able to produce walk (region W), trot (region T) and bound (region B). These brute-force bifurcation diagrams have been obtained by using CEPAGE to simulate the CPG by increasing (black lines) and decreasing (gray lines) α values. The comparison points out the presence of a bistability interval between regions T and B. The corresponding membrane voltages $V_i(t)$ for the flexor cells over a window of 600ms are shown in the bottom panels, where the color code is the same as for the cells in Fig. 2.

Figure 5 shows how the bifurcation diagram for $\Delta\phi_{12}$ changes by removing some synaptic connections. These results are coherent with biophysical experiments where some CPG cells are genetically ablated [43] and are completely similar to those obtained in [28] for the 40-cell CPG.

Because in our reduced model the cells removed in the original 40-cell CPG are no longer included, we modified the synaptic efficacies as follows (the reader not familiar with

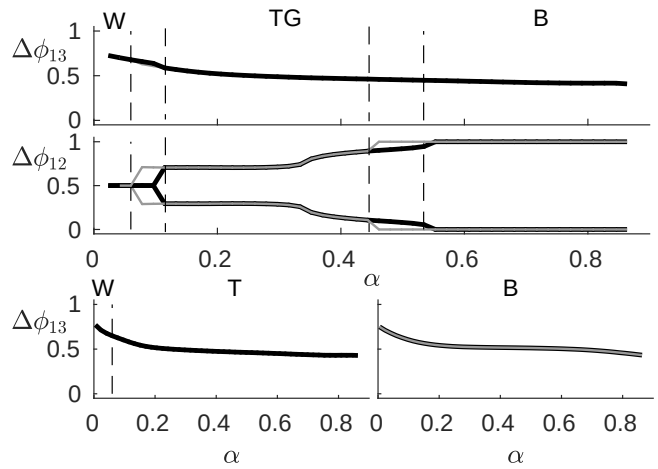

Fig. 5. Stable phase differences/lags $\Delta\varphi_{12}$ and $\Delta\varphi_{13}$ in the 8-cell CPG. Upper panels: ablation of cell $V0_V$ in the original 40-cell CPG. Bottom-left panel: ablation of cells $V0_D$ and $V0_V$. Bottom-right panel: ablation of cell $V3$. For the bottom panels, $\Delta\varphi_{12}$ remains constant at 0 (left) and 0.5 (right).

physiological details is referred to [28] for deeper insights about the removed cells/connections):

- $V0_V$: we decreased the synaptic efficacies of the inhibitory connections between the flexor cells 1-2 and 3-4, since the cell $V0_V$ in the 40-cell CPG is involved in one of the two possible inhibitory connections (the other connection involves the cell $V0_D$) between the considered flexor cells.
- $V0_D$ and $V0_V$: we removed the inhibitory connections between the flexor cells 1-2 and 3-4, for the reasons explained above.
- $V3$: we removed the excitatory connections between the flexor cells 1-2 and 3-4, for similar reasons.

In the upper panels, due to the lower strength of the inhibitory connections between left and right flexor cells, region T disappears, whereas region B is larger than in Fig. 4. Moreover, region TG appears, meaning that the quadruped can generate a transverse gallop gait. Black and gray lines have the same meaning as in Fig. 4 and reveal the presence of bistability in two transition regions.

In the last two cases the interpretation is quite direct: due to the absence of inhibitory (excitatory) connections between left side and right side, the CPG is able to generate only in-phase (anti-phase) patterns. This prevents the quadruped from producing bound (bottom-left panel) or walk and trot (bottom-right panel).

Summarizing, our analysis shows that the 8-cell CPG has the same behaviors as the 40-cell CPG and can produce up to four gaits (only three if we keep unchanged the CPG structure), among those listed in Tab. I. Now, we want to see if it is possible obtaining all the five gaits listed in the table, by taking the CPG structure fixed and acting only on the way g_{ij}^{ex} and D_i depend on the brain-stem parameter α. So, after an analysis problem, now we face a design problem, following the steps described in Sec. III.

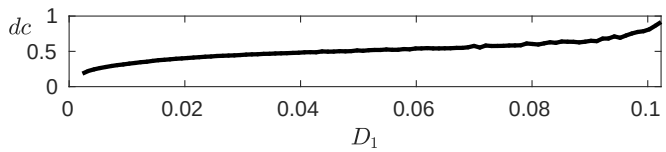

Fig. 6. Step 1 (see the gray dashed rectangle in Fig. 2): asymptotic duty cycle **dc** of the fore flexor cell vs. $\mathbf{D_1}$.

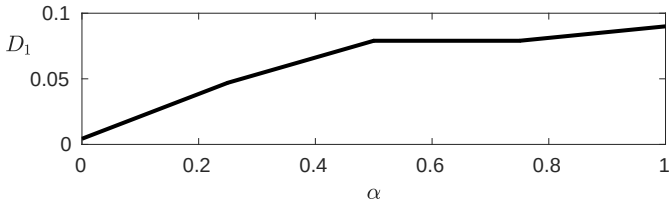

Fig. 7. Step 1: the chosen PWL function $\mathbf{D_1(\alpha)}$.

B. Step 1

We analyze a fore flexor-extensor pair (see the gray dashed rectangle in Fig. 2). Figure 6 shows the asymptotic flexor cell duty cycle vs. parameter D_1 (see Appendix A, last equation of system (5)) of the same cell.

The minimum and maximum dc values we want to generate are 0.25 (walk) and 0.65 (bound). Then D_1 can range between 0.0043 and 0.09 and we define it as a non-decreasing PWL function $D_1(\alpha)$. This choice allows obtaining the same duty cycle for different values of α and, consequently, we can obtain different gaits sharing the same duty cycle. Figure 7 shows the chosen function $D_1(\alpha)$ in the considered example.

C. Step 2

We analyze the sub-structure within the gray solid box in Fig. 2, where the fore flexor-extensor pairs are identical. Through CEPAGE, we carry out a two-dimensional bifurcation analysis of the stable phase difference $\Delta\phi_{12}$ with respect to α and g^{ex} ($= g^{ex}_{12} = g^{ex}_{21}$). Figure 8 shows the obtained brute-force bifurcation diagram.

In the blue region, the (unique) stable equilibrium point has a phase coordinate $\Delta\phi_{12} = 0$ (in-phase). In the yellow region, the (unique) stable equilibrium point has a locked phase $\Delta\phi_{12} = 0.5$ (anti-phase). In the third intermediate region, instead, two stable equilibria coexist; the diagram shows the one with phase $0 < \Delta\phi_{12} < 0.5$. The second equilibrium (not shown) has phase $1 - \Delta\phi_{12}$. This is the reason because of the diagram colorbar ranging from 0 through 0.5. On the whole, we can obtain any phase difference between 0 and 1. The red curves mark supercritical pitchfork bifurcations, obtained again through CEPAGE (brute-force approach).

We remark that, despite the fact that the presence of bistability makes the produced patterns less robust, for the asymmetric gaits we can obtain mono-stability by breaking the symmetry, as we will see below. For the symmetric gaits, the bistability just means that the limbs move in the reverse order, but the gait remains the same.

At this point, we can define a function $g^{ex}(\alpha)$ so as to have a continuous sequence of gaits. The chosen function is shown in Fig. 8 (black PWL curve).

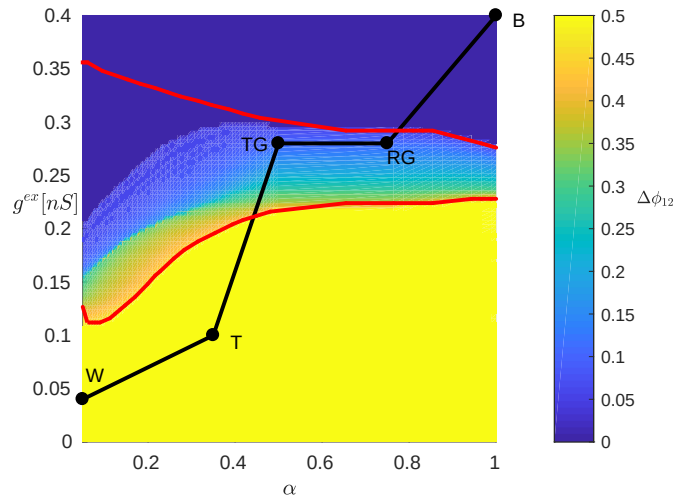

Fig. 8. (Color online) Step 2 (see the gray solid box in Fig. 2): brute-force bifurcation diagram in the parameter plane (α,g^{ex}). Red curves: supercritical pitchfork bifurcations. Black dots: chosen parameter pairs corresponding to five different gaits. Black line: chosen path to obtain the sequence of gaits.

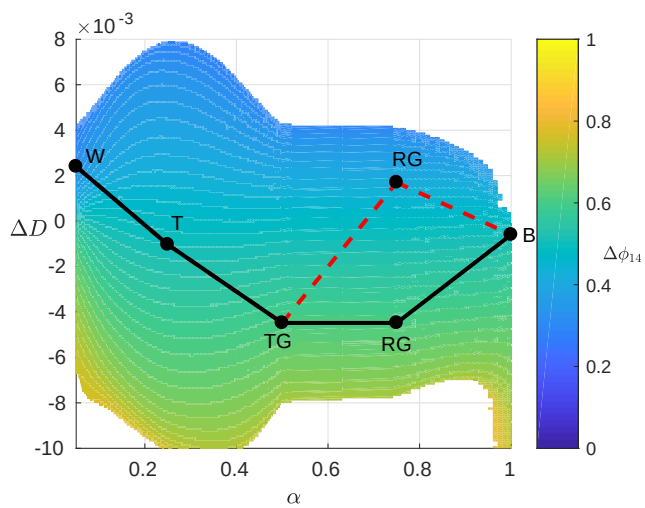

Fig. 9. (Color online) Step 3 (see the black dashed box in Fig. 2): brute-force bifurcation diagram in the parameter plane (α,ΔD). Black dots: chosen parameter pairs corresponding to five different gaits. The white pixels denote parameter pairs corresponding to a quiescent behavior of the cell (no spiking occurs at regime). Chosen PWL functions $\Delta D_3(\alpha)$ (solid black line) and $\Delta D_4(\alpha)$ (dashed red line).

D. Step 3

Step 3 is related to the analysis of the CPG sub-network within the black dashed box in Fig. 2. Cell 1 depends on α through $D_1(\alpha)$, whereas cell 4 initially depends on two parameters through $D_4(\alpha, \Delta D) = D_1(\alpha) + \Delta D$.

CEPAGE provided the 2D bifurcation diagram shown in Fig. 9 for the equilibrium values of $\Delta\phi_{14}$ with respect to α and ΔD. By properly choosing ΔD as a PWL function of α connecting the values selected at the end of Step 1 (marked by black dots), we can obtain a function $\Delta D_4(\alpha)$ ensuring the desired phase lags $\Delta\phi_{14}$ between fore and hind legs.

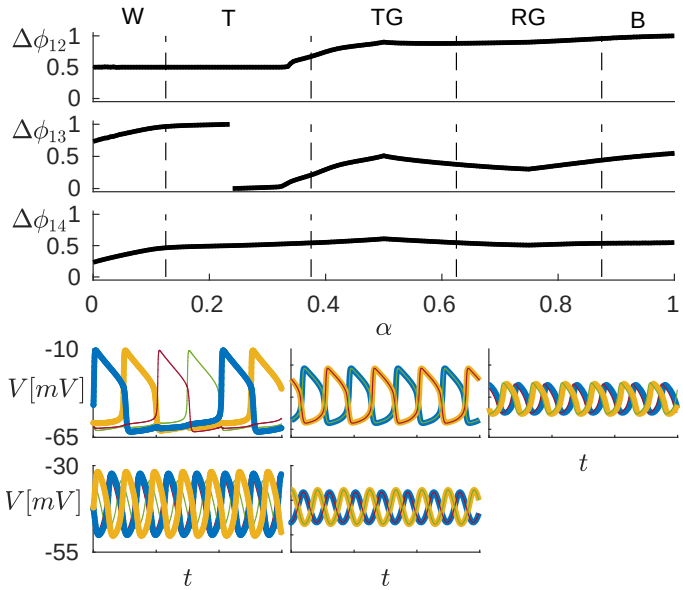

Fig. 10. (Color online) Upper panels: 1D bifurcation diagrams obtained by applying to the whole CPG the chosen functions of α, providing the sequence of gaits walk (region W), trot (T), transverse gallop (TG), rotary gallop (RG), bound (B). Bottom panels: membrane voltages $V_i(t)$ for the flexor cells in the five regions, over a window of 600ms (color code as for the cells in Fig. 2).

If we want to obtain symmetric gaits only, we can design the right part of the CPG as identical to the analyzed subnetwork. On the contrary, if we want to obtain also asymmetric gaits, we have to design differently the two sides. In particular, in this case study, we can define two functions $\Delta D_3(\alpha)$ and $\Delta D_4(\alpha)$ (one for each side, right/left) so as to have a continuous sequence of gaits. The chosen functions are shown in Fig. 9: the dashed red line is related to the left legs and the black solid line to the right legs.

E. Step 4

Finally, we check the designed CPG by carrying out the same bifurcation analysis as in Fig. 4, by setting $g^{ex}_{12} = g^{ex}_{21} = g^{ex}_{34} = g^{ex}_{43} = g^{ex}(\alpha)$, $D_2(\alpha) = D_1(\alpha)$, $D_3(\alpha) = D_1(\alpha) + \Delta D_3(\alpha)$ and $D_4(\alpha) = D_1(\alpha) + \Delta D_4(\alpha)$, by using the PWL functions of α obtained through the previous steps. The result is shown in Fig. 10. The upper panels show the bifurcation diagrams obtained by applying the chosen functions and point out the correct sequence of gaits. The bottom panels show the corresponding evolution of the steady-state membrane voltages $V_i(t)$ for the flexor cells in the five regions, over a window of 600ms and with voltages ranging in the interval $[-60, -10]$mV (the color code is the same as for the cells in Fig. 2). As pointed out in Sec. III, each voltage has its own duty cycle, amplitude, frequency, and phase, which determine on the whole the corresponding gait.

V. Case study 2: a synthetic CPG

In this section we show how to design a 4-cell purely synthetic CPG in order to generate the same gaits as before.

The chosen neuron model is the modified FitzHugh-Nagumo model described in [21] and reported in Appendix B for ease of reference. In this model, all variables are normalized and dimensionless.

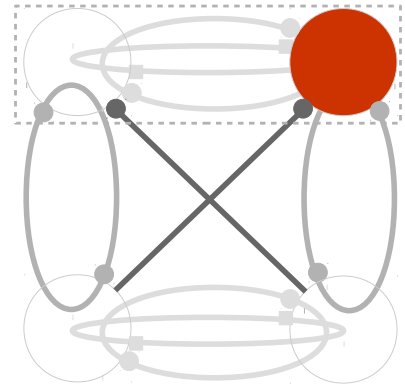

Fig. 11. (Color online) 4-unit synthetic CPG. Gray dashed box: half-center oscillator (see step 1) with standard inhibitory synaptic connections (filled circles) and additional excitatory synaptic connections (filled squares). The CPG is completed by the mid-gray (see step 2) and dark-gray (see step 3) inhibitory connections.

We use the synapse model (2), with $\nu = 0.3$, $\theta = 0$, $E_{in} = -1.5$ and $E_{ex} = 1$.

In this case, we consider only the phase relationships between limbs for each gait, i.e., we focus on the times of "maximum contact" between limb and ground. For the sake of simplicity, in this example we neglect the duty cycle, which accounts for the duration of the contact. In other words, this network is only a rhythm generator, that would require either a more complex cell model or further cells (e.g., a pattern formation network and motor neurons, as proposed in [44]) to become a realistic CPG, able to modulate also duty cycles, amplitudes and frequencies of the cells driving flexor and extensor muscles. With this *caveat* in mind, henceforth the network will be called anyway CPG.

Our goal in this second case study is to design a synthetic CPG that, for a given parameter setting, produces only one stable motif, in order to ensure robustness for the generated pattern.

Some synapses are fixed whereas others depend on the bifurcation parameter α □ $[0, 1]$, in order to make the CPG able to switch between the desired gaits.

The complete CPG reference structure is shown in Fig. 11. Actually, the design strategy starts from a simpler block, i.e., the HCO within the gray dashed box. With respect to a standard HCO (containing only inhibitory synapses, light-gray connections ending with filled circles), here we add also excitatory synapses (ending with filled squares), whose strengths g^{ex}_{ij} depend on α.

The second step in the design involves two HCOs (made up of cells 1-2 and 3-4), that are connected through the vertical gray inhibitory synapses.

Step 3 involves also the dark-gray inhibitory (or excitatory) synapses, whose strengths g^{in}_{ij} depend on α. Each step requires some analysis (carried out with CEPAGE), which is described in detail in the following.

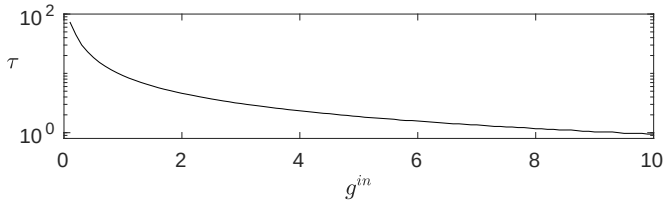

Fig. 12. Maximum convergence time of the phase difference $\Delta\varphi_{12}$ to the equilibrium point in the HCO for $g_{12}^{ex} = g_{21}^{ex} = 0$.

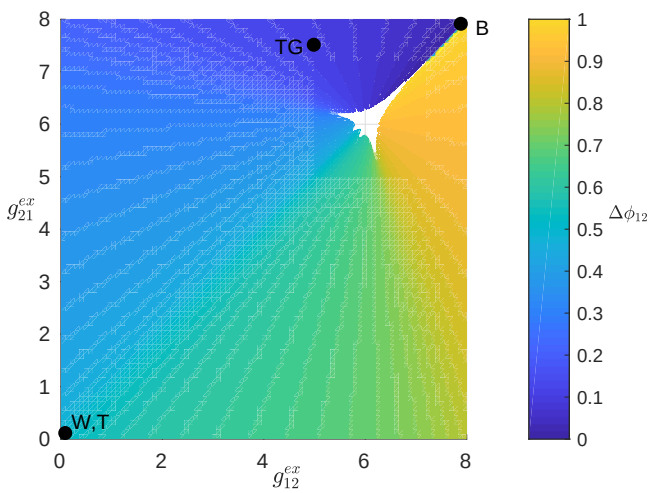

Fig. 13. (Color online) Step 1: two-dimensional bifurcation diagram for the excitatory synaptic efficacies of the HCO (gray dashed box in Fig. 11).

A. Step 1

First of all, we set the strength of the inhibitory synapses, which will be taken as a reference for the whole design process. Since the HCO has always a stable equilibrium point for the phase difference, we can set the synaptic efficacy g^{in} (the same for both connections $1 \rightarrow 2$ and $2 \rightarrow 1$) according to the desired convergence time scale. Figure 12 shows the maximum convergence time of the phase difference $\Delta\phi_{12}$ to the equilibrium point for $g_{12}^{ex} = g_{21}^{ex} = 0$. We choose $g^{in} = 4$ in order to have convergence times in the scale of some normalized units of time.

Now, we have to set the strengths of the excitatory synapses. To this end, we obtain a two-dimensional bifurcation diagram showing the equilibrium phase difference $\Delta\phi_{12}$ with respect to g_{12}^{ex} and g_{21}^{ex} (see Fig. 13). White pixels mark the presence of multiple stable equilibria. The white region is due to the presence of a subcritical pitchfork bifurcation along the main diagonal, which degenerates in a fold bifurcation outside the diagonal (due to symmetry breaking).

Points W/T, TG, B in the figure mark the pairs chosen to reproduce different gaits with the complete CPG, on the basis of the corresponding left-right phase difference (see Table I): walk and trot (W/T, anti-phase LR alternation), bound (B, in-phase LR alternation), transverse gallop (TG, almost in-phase LR alternation). Figure 14 shows the chosen functions $g_{12}^{ex}(\alpha)$ (black solid line) and $g_{21}^{ex}(\alpha)$ (gray dashed line).

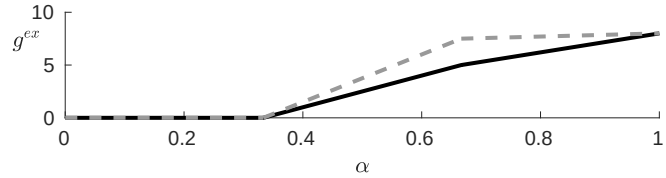

Fig. 14. Step 1: chosen PWL functions $g_{12}^{ex}(\alpha)$ (black solid line) and $g_{21}^{ex}(\alpha)$ (gray dashed line).

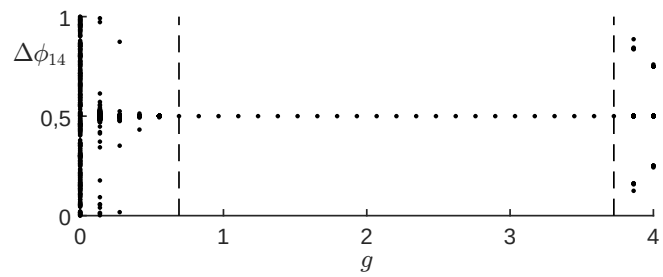

Fig. 15. Step 2: asymptotic values of the phase difference $\Delta\varphi_{14}$ with respect to g.

B. Step 2

The bottom HCO is identical to the top one, with g_{12}^{ex} and g_{21}^{ex} set to point A, in order to have left-right alternation with $\Delta\phi_{12} = 0.5$. Here, we analyze the CPG behavior changes with respect to the strength g of the 4 mid-gray inhibitory synapses shown in Fig. 11.

The 1D bifurcation diagram in Fig. 15 shows the equilibrium value of the phase difference $\Delta\phi_{14}$ with respect to g. The bifurcation diagram contains three regions, whose edges are marked by dashed vertical lines. In the left region there is no phase locking (i.e., the CPG works out of an Arnold tongue), due to the too low value of g. In the right region, the g strength approaches $g^{in} = 4$ and further stable equilibria appear, thus producing undesired multi-stability.

Then we set g to a value within the central region. In order to ensure structural stability, we choose $g = 2$.

C. Step 3

Now we want to set the strength g_c of the two dark-gray inhibitory synapses shown in Fig. 11 in order to generate all the desired front-hind alternations, corresponding to different rhythms.

To this end, Fig. 16 provides one-dimensional bifurcation diagrams showing the stable equilibrium phase differences $\Delta\phi_{12}$ and $\Delta\phi_{14}$ with respect to g_c, for the HCO configured in the points W,T (black lines), TG (gray lines), B (light-gray lines) in Fig. 13.

We want to ensure that g_c is set to a value that (i) does not alter the existing LR phase difference and (ii) provides the desired FH phase difference. The upper bifurcation diagram in Fig. 16 shows the actual stable equilibrium phase differences $\Delta\phi_{12}$ versus g_c (solid lines) and those set during step 1 (cross markers). It is evident that for the parameter settings W,T and TG the desired equilibrium value of $\Delta\phi_{12}$ is kept for any g_c, whereas for the parameter setting B only g_c values lower

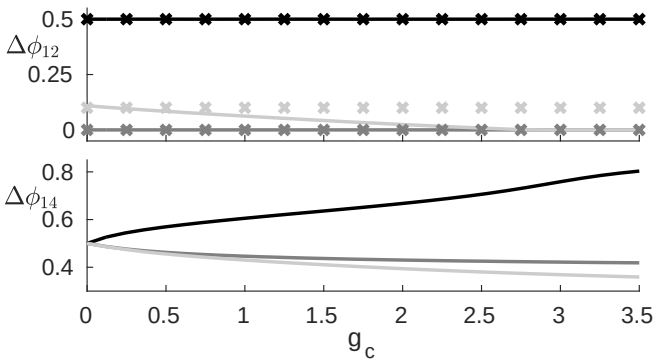

Fig. 16. Step 3: one-dimensional bifurcation diagram showing the stable equilibria with respect to g_c in the case of inhibitory synapses.

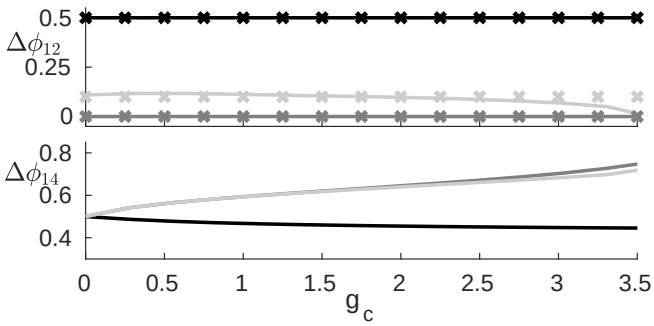

Fig. 17. Step 3: one-dimensional bifurcation diagram showing the stable equilibria with respect to g_c in the case of excitatory synapses.

than about 0.2 allow keeping the desired equilibrium value of $\Delta\phi_{12}$.

About condition (ii), from the lower bifurcation diagram we deduce that for the parameter setting W,T (black line) we can only have a delay between fore and hind limbs ($\Delta\phi_{14} > 0.5$) and acting on g_c we can control this delay over a reasonable interval (with $\Delta\phi_{14}$ ranging from 0.5 to about 0.8). On the contrary, for the other two settings we can only have an advance of the fore limb with respect to the hind limb ($\Delta\phi_{14} < 0.5$) and acting on g_c we can control this delay over a small interval (with $\Delta\phi_{14}$ ranging from about 0.4 to 0.5).

If the nature of the synaptic connections is changed to excitatory, we obtain the bifurcation diagrams shown in Fig. 17. A direct comparison of Figs. 16 and 17 makes it evident that the two kinds of connections have a complementary effect. This suggests that in the case W,T inhibitory connections can be favorably used to obtain a prescribed delay between fore and hind limbs, whereas excitatory connections are better to obtain a prescribed advance. Similarly, in the cases TG and B inhibitory (excitatory) connections can be used to obtain a prescribed advance (delay).

Among the allowed g_c values, we choose the one corresponding to the equilibrium value of $\Delta\phi_{14}$ closest to the desired rhythm (see Table I), thus obtaining the functions $g^{in}_{13}(\alpha) = g^{in}_{24}(\alpha)$ (black solid curve) and $g^{ex}_{13}(\alpha) = g^{ex}_{24}(\alpha)$ (gray dashed curve) shown in Fig. 18.

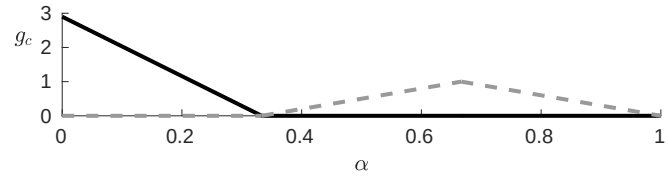

Fig. 18. Step 3: chosen PWL functions $g_c(\alpha)$ in the case of inhibitory (black solid line) or excitatory (gray dashed line) synapses.

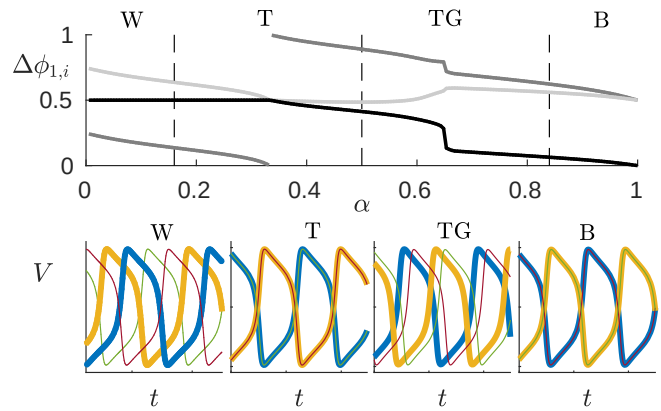

Fig. 19. (Color online) Step 3 (see text). Upper panel: 1D bifurcation diagrams obtained by applying to the whole CPG the chosen functions of α, providing the sequence of rhythms walk (region W), trot (T), transverse gallop (TG), bound (B). Bottom panels: normalized membrane voltages $V_i(t)$ for the CPG cells in the four regions, ranging in the interval $[-1, 1]$ over a window of 50 units of time (color code as for the cells in Fig. 11).

D. Step 4

Figure 19 shows the stable equilibrium values of the phase differences (upper panel) and the time evolution of the normalized membrane voltages (lower panels) by changing α to obtain the desired rhythms: walk (region W), trot (T), transverse gallop (TG) and bound (B).

The width of the time axes in the lower panels is 50 units of time (notice that the model used in this case study, described in Appendix B, is normalized and uses dimensionless variables).

E. Asymmetric rhythms

If we want to add to the rhythm sequence also asymmetric rhythms, the procedure described for step 3 in the case of symmetric rhythms must change. In the complete CPG, cells 1 and 2 are initially assumed to be not connected, in order to avoid LR synchronization, whereas cells 3 and 4 remain connected through the synapses with PWL functions $g^{ex}_{34}(\alpha) = g^{ex}_{12}(\alpha)$ and $g^{ex}_{43}(\alpha) = g^{ex}_{21}(\alpha)$ (see Fig. 14).

Now we obtain again a bifurcation diagram with respect to g_c (as in Figs. 17 and 18), to choose proper values of g_c and a proper PWL function $g_c(\alpha)$.

Finally, we choose proper values of g^{ex}_{12} and g^{ex}_{21} (as in Fig. 13) and related PWL functions $g^{ex}_{12}(\alpha)$ and $g^{ex}_{21}(\alpha)$ (as in Fig. 14), by keeping unchanged $g^{ex}_{34}(\alpha)$ and $g^{ex}_{43}(\alpha)$.

Figure 20 shows the stable equilibrium values of the phase differences (upper panel) and the time evolution of the neuron voltages (lower panels) by changing α to obtain the desired

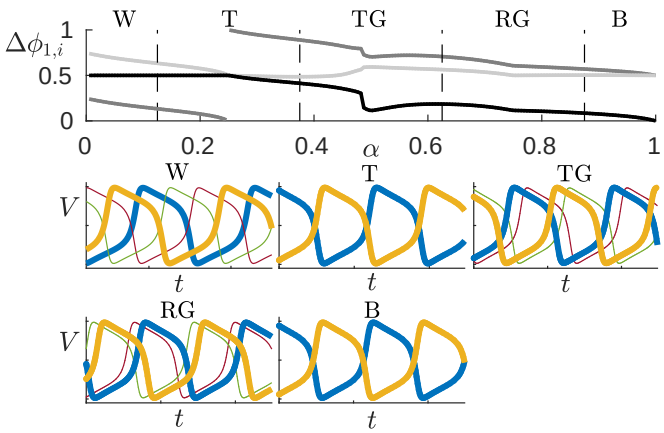

Fig. 20. (Color online) Step 3 for asymmetric rhythms (see text). Upper panel: 1D bifurcation diagrams obtained by applying to the whole CPG the chosen functions of α, providing the sequence of rhythms walk (region W), trot (T), transverse gallop (TG), rotary gallop (RG), bound (B). Bottom panels: normalized membrane voltages $V_i(t)$ for the CPG cells in the four regions, ranging in the interval $[-1, 1]$ over a window of 50 units of time (color code as for the cells in Fig. 11).

rhythms: walk (region W), trot (T), transverse gallop (TG), rotary gallop (RG), and bound (B).

We remark once more that in this case (contrary to the first case study), we focused on the phase differences only, since amplitudes, frequencies and duty cycles of the cell voltages can be properly modulated only by using a more complete CPG model. Inasmuch as this paper is focused on the design method, the cell model was used as is and the method was applied in order to make the CPG generate the correct phase differences. This is the reason why in this case the voltages $V_i(t)$ differ in the phase only.

VI. Concluding remarks

While papers devoted to the analysis of CPGs are quite common in the scientific literature, there is a lack of papers mainly focused on their design. This paper aimed to bridge this gap, focusing on the case of locomotion control of quadrupeds. The main features of the proposed design strategy can be summarized as follows:

- parallel development of analysis and design, based on multi-parameter bifurcation theory;
- combination of local analysis (and related design of some local properties/parameters of the CPG) and global analysis, to ensure structural stability of the overall system;
- use of a bifurcation parameter modeling the brain-stem drive coming from the supra-spinal networks to properly govern gait transitions through the nonlinear functions $g_{ij}^{ex}(\alpha)$.

The method has been applied to model with relatively simple dynamical networks either a real structure (first case study, reduced-complexity version of a bio-inspired CPG) or just specific quadrupeds' functionalities (second case study, synthetic CPG), by resorting to the toolbox CEPAGE for efficient numerical analysis. After proper robustness analysis with respect to cell and synapse models and after properly relating the parameter α to sensory inputs (in order to introduce also an effective closed-loop control, besides the open-loop control provided by the CPG), the obtained results can find applications in the fields of bio-robotics [23], [24] and rehabilitation [25], [26]. Moreover, we will have to introduce a direct sensory feedback to properly adjust the gait in the presence of mechanical perturbations, for instance, if one leg cannot find a foothold [45], [46].

To conclude, we briefly address the physical implementation problem related to applications. As pointed out in [12], a CPG-based locomotion control is usually programmed in software and running on hardware (microcontroller, DSP, FPGA or dedicated hardware). Providing an overview on possible hardware implementations, which (except purely digital solutions) depend on the specific choice of cell and synapse models, is out of the scope of this paper. About this issue, the reader is kindly referred to surveys such as [12], [47] or to specific studies related to the cited applications [48], [49].

Acknowledgments

MS would like to thank his colleague and friend Federico Bizzarri for stimulating discussions. The authors also thank Simon Danner for providing benchmark results for case study 1.

Appendix A
Case study 1

The model employed in the first case study is [28]

$$
\begin{aligned}
C\frac{dV_i}{dt} &= -I_{Na} - I_L - I_D^{(i)}(\alpha) + I_{syn}^{(i)} \\
\tau\frac{dh}{dt} &= h_\infty - h \\
I_L &= g_L \cdot (V_i - E_L) \\
I_{Na} &= g_{Na} \cdot m \cdot h \cdot (V_i - E_{Na}) \\
m &= \left(1 + e^{\frac{V_i - V_m}{k_m}}\right)^{-1} \\
h_\infty &= \left(1 + e^{\frac{V_i - V_h}{k_h}}\right)^{-1} \\
\tau &= \tau_0 + \frac{\tau_M - \tau_0}{cosh\left(\frac{V_i - V_\tau}{k_\tau}\right)} \\
I_D^{(i)}(\alpha) &= g_D \cdot D_i(\alpha) \cdot (V_i - E_{ex})
\end{aligned}
\tag{5}
$$

where $C = 10$pF, $g_L = 4.5$nS, $E_L = -62.5$mV, $g_{Na} = 4.5$nS, $E_{Na} = 50$mV, $V_m = -40$mV, $k_m = -6$mV, $V_h = -45$mV, $k_h = 4$mV, $\tau_0 = 80$ms, $\tau_M = 160$ms, $V_\tau = -35$mV, $k_\tau = 15$mV and $g_D = 10$nS, $D_5 = D_6 = D_7 = D_8 = 0.1$, $D_1 = D_2 = 0.1\alpha + 0.0023$ and $D_3 = D_4 = 0.104\alpha + 0.0010$

The synapses parameters are $\nu = 0.3mV^{-1}$, $\theta = -30mV$, $E_{ex} = -10mV$ and $E_{in} = -75mV$, whereas the constant synaptic strengths are listed in Tab. II.

The synaptic strengths of the excitatory synapses depend on

TABLE II
SYNAPSES EFFICACIES OF THE 8-CELL CPG.

Connections	value [nS]
g^{in}_{15}, g^{in}_{26} , g^{in}_{37}, g^{in}_{48}	**0.228**
g^{in}_{51}, g^{in}_{62}, g^{in}_{73}, g^{in}_{84}	**2.853**
g^{in}_{16}, g^{in}_{25}, g^{in}_{83}, g^{in}_{74}	**0.0221**
g^{in}_{12}, g^{in}_{21}	**0.298**
g^{in}_{34}, g^{in}_{43}	**0.448**
g^{in}_{41}, g^{in}_{32}	**0.1272**
g^{in}_{41}, g^{in}_{32}	**0.0545**

α as follows:

$$\begin{aligned} g^{ex}_{12}(\alpha) = g^{ex}_{21}(\alpha) &= 115.98\alpha^{10} - 231.71\alpha^{9} + 25.54\alpha^{8} \\ &+329.37\alpha^{7} - 407.13\alpha^{6} + 235.88\alpha^{5} - 76.053\alpha^{4} \\ &+13.751\alpha^{3} - 1.1155\alpha^{2} + 0.11545\alpha + 0.16808 \\ g^{ex}_{34}(\alpha) = g^{ex}_{43}(\alpha) &= 3058.8\alpha^{10} - 13011\alpha^{9} + 23662\alpha^{8} \\ &-23916\alpha^{7} + 14651\alpha^{6} - 5568.3\alpha^{5} + 1292\alpha^{4} \\ &-172.9\alpha^{3} + 12.005\alpha^{2} - 0.25126\alpha + 0.1689 \end{aligned} \tag{6}$$

APPENDIX B
CASE STUDY 2

The model used in the second case study is [21]

$$\begin{aligned} \frac{dV_i}{dt} &= V_i - V_i^3 - x_i + I + \beta I^{(i)}_{syn} \\ \frac{dx_i}{dt} &= \epsilon \frac{1}{1 - e^{-10V_i}} - x_i \end{aligned} \tag{7}$$

where $I = 0.5$, $\beta = 10^{-3}$ and $\epsilon = 0.3$.

REFERENCES

[1] M. Goulding, "Circuits controlling vertebrate locomotion: moving in a new direction," *Nature Reviews Neuroscience*, vol. 10, no. 7, pp. 507–518, 2009.

[2] K. L. Briggman and W. B. Kristan, "Imaging dedicated and multifunctional neural circuits generating distinct behaviors." *J. Neurosci.*, vol. 26, no. 42, pp. 10 925–10 933, Oct 2006. [Online]. Available: http://dx.doi.org/10.1523/JNEUROSCI.3265-06.2006

[3] S. Grillner and T. M. Jessell, "Measured motion: searching for simplicity in spinal locomotor networks," *Current opinion in neurobiology*, vol. 19, no. 6, pp. 572–586, 2009.

[4] O. Kiehn, "Decoding the organization of spinal circuits that control locomotion," *Nature Reviews Neuroscience*, 2016.

[5] A. Sakurai and P. S. Katz, "Functional recovery after lesion of a central pattern generator." *J. Neurosci.*, vol. 29, no. 42, pp. 13 115–13 125, Oct 2009. [Online]. Available: http://dx.doi.org/10.1523/JNEUROSCI.3485-09.2009

[6] A. I. Selverston, "Invertebrate central pattern generator circuits." *Philos. T. R. Soc. Lond. B*, vol. 365, no. 1551, pp. 2329–2345, Aug 2010. [Online]. Available: http://dx.doi.org/10.1098/rstb.2009.0270

[7] P. S. Katz, "Neural mechanisms underlying the evolvability of behaviour." *Philos. T. R. Soc. B*, vol. 366, no. 1574, pp. 2086–2099, Jul 2011. [Online]. Available: http://dx.doi.org/10.1098/rstb.2010.0336

[8] S. Grillner, "Biological pattern generation: the cellular and computational logic of networks in motion," *Neuron*, vol. 52, no. 5, pp. 751–766, 2006.

[9] L. M. Jordan, "Initiation of locomotion in mammals," *Annals of the New York Academy of Sciences*, vol. 860, no. 1, pp. 83–93, 1998.

[10] L. M. Jordan, J. Liu, P. B. Hedlund, T. Akay, and K. G. Pearson, "Descending command systems for the initiation of locomotion in mammals," *Brain research reviews*, vol. 57, no. 1, pp. 183–191, 2008.

[11] S. Rossignol, R. Dubuc, and J.-P. Gossard, "Dynamic sensorimotor interactions in locomotion," *Physiological reviews*, vol. 86, no. 1, pp. 89–154, 2006.

[12] J. Yu, M. Tan, J. Chen, and J. Zhang, "A survey on CPG-inspired control models and system implementation," *IEEE Transactions on neural networks and learning systems*, vol. 25, no. 3, pp. 441–456, 2014.

[13] S. Jalil, D. Allen, J. Youker, and A. Shilnikov, "Toward robust phase-locking in melibe swim central pattern generator models," *Chaos: An Interdisciplinary Journal of Nonlinear Science*, vol. 23, no. 4, p. 046105, 2013.

[14] J. Wojcik, R. Clewley, and A. Shilnikov, "Order parameter for bursting polyrhythms in multifunctional central pattern generators," *Phys. Rev. E*, vol. 83, no. 5, p. 056209, 2011.

[15] J. T. C. Schwabedal, A. B. Neiman, and A. L. Shilnikov, "Robust design of polyrhythmic neural circuits." *Phys. Rev. E*, vol. 90, no. 2, p. 022715, Aug 2014.

[16] J. Wojcik, J. Schwabedal, R. Clewley, and A. L. Shilnikov, "Key bifurcations of bursting polyrhythms in 3-cell central pattern generators," *PloS One*, vol. 9, no. 4, p. e92918, 2014.

[17] A. Kozlov, M. Huss, A. Lansner, J. H. Kotaleski, and S. Grillner, "Simple cellular and network control principles govern complex patterns of motor behavior," *Proceedings of the National Academy of Sciences*, vol. 106, no. 47, pp. 20 027–20 032, 2009.

[18] M. Golubitsky, I. Stewart, P.-L. Buono, and J. Collins, "Symmetry in locomotor central pattern generators and animal gaits," *Nature*, vol. 401, no. 6754, pp. 693–695, 1999.

[19] L. P. Shilnikov, A. L. Shilnikov, D. V. Turaev, and L. O. Chua, *Methods of qualitative theory in nonlinear dynamics. Volume I*. World Scientific, 1998, vol. 5.

[20] L. P. Shilnikov, A. L. Shilnikov, D. V. Turaev, and L. O. Chua, *Methods of qualitative theory in nonlinear dynamics. Volume II*. World Scientific, 2001, vol. 5.

[21] J. Schwabedal, D. Knapper, and A. Shilnikov, "Qualitative and quantitative stability analysis of penta-rhythmic circuits," *Nonlinearity*, no. 39, p. 647"3676, 2016.

[22] F. Li, A. Basu, C.-H. Chang, and A. H. Cohen, "Dynamical systems guided design and analysis of silicon oscillators for central pattern generators," *IEEE Transactions on Circuits and Systems I: Regular Papers*, vol. 59, no. 12, pp. 3046–3059, 2012.

[23] A. J. Ijspeert, "Central pattern generators for locomotion control in animals and robots: a review," *Neural Networks*, vol. 21, no. 4, pp. 642–653, 2008.

[24] Y. Hu, J. Liang, and T. Wang, "Parameter synthesis of coupled nonlinear oscillators for CPG-based robotic locomotion," *IEEE Transactions on Industrial Electronics*, vol. 61, no. 11, pp. 6183–6191, 2014.

[25] K. A. Mazurek, B. J. Holinski, D. G. Everaert, V. K. Mushahwar, and R. Etienne-Cummings, "A mixed-signal VLSI system for producing temporally adapting intraspinal microstimulation patterns for locomotion," *IEEE transactions on biomedical circuits and systems*, vol. 10, no. 4, pp. 902–911, 2016.

[26] J. A. Bamford, R. M. Lebel, K. Parseyan, and V. K. Mushahwar, "The fabrication, implantation, and stability of intraspinal microwire arrays in the spinal cord of cat and rat," *IEEE Transactions on Neural Systems and Rehabilitation Engineering*, vol. 25, no. 3, pp. 287–296, 2017.

[27] M. Lodi, A. Shilnikov, and M. Storace, "CEPAGE: a toolbox for central pattern generator analysis," in *2017 IEEE International Symposium on Circuits and Systems (ISCAS)*, May 28–31 2017, pp. 1–4.

[28] S. M. Danner, S. D. Wilshin, N. A. Shevtsova, and I. A. Rybak, "Central control of interlimb coordination and speed-dependent gait expression in quadrupeds," *The Journal of physiology*, vol. 594, no. 23, pp. 6947–6967, 2016.

[29] D. Somers and N. Kopell, "Rapid synchronization through fast threshold modulation," *Biological cybernetics*, vol. 68, no. 5, pp. 393–407, 1993.

[30] L. Zhao and A. Nogaret, "Experimental observation of multistability and dynamic attractors in silicon central pattern generators," *Physical Review E*, vol. 92, no. 5, p. 052910, 2015.

[31] R. Barrio, M. Rodríguez, S. Serrano, and A. Shilnikov, "Mechanism of quasi-periodic lag jitter in bursting rhythms by a neuronal network," *EPL (Europhysics Letters)*, vol. 112, no. 3, p. 38002, 2015.

[32] J. Schwabedal, D. Knapper, K. Pusuluri, and D. Alacam. Motiftoolbox. [Online]. Available: https://github.com/jusjusjus/Motiftoolbox

[33] E. J. Doedel, "AUTO: A program for the automatic bifurcation analysis of autonomous systems," *Congr. Numer*, vol. 30, pp. 265–284, 1981.

[34] A. Dhooge, W. Govaerts, and Y. A. Kuznetsov, "MATCONT: a MATLAB package for numerical bifurcation analysis of ODEs," *ACM Transactions on Mathematical Software (TOMS)*, vol. 29, no. 2, pp. 141–164, 2003.

[35] D. Linaro and M. Storace, "BAL: A library for the brute-force analysis of dynamical systems," *Computer Physics Communications*, vol. 201, pp. 126–134, 2016.

[36] V. Novičenko and K. Pyragas, "Computation of phase response curves via a direct method adapted to infinitesimal perturbations," *Nonlinear Dynamics*, vol. 67, no. 1, pp. 517–526, 2012.

[37] W. E. Sherwood, R. Harris-Warrick, and J. Guckenheimer, "Synaptic patterning of left-right alternation in a computational model of the rodent hindlimb central pattern generator," *Journal of computational neuroscience*, vol. 30, no. 2, pp. 323–360, 2011.

[38] R. H. Lee and C. Heckman, "Adjustable amplification of synaptic input in the dendrites of spinal motoneurons in vivo," *Journal of Neuroscience*, vol. 20, no. 17, pp. 6734–6740, 2000.

[39] P. Meyrand, J. Simmers, and M. Moulins, "Construction of a pattern-generating circuit with neurons of different networks," *Nature*, vol. 351, no. 6321, p. 60, 1991.

[40] W. B. Kristan, R. L. Calabrese, and W. O. Friesen, "Neuronal control of leech behavior," *Progress in neurobiology*, vol. 76, no. 5, pp. 279–327, 2005.

[41] K. L. Briggman, H. D. Abarbanel, and W. B. Kristan, "Optical imaging of neuronal populations during decision-making," *Science*, vol. 307, no. 5711, pp. 896–901, 2005.

[42] A. Berkowitz, "Physiology and morphology of shared and specialized spinal interneurons for locomotion and scratching," *Journal of neurophysiology*, vol. 99, no. 6, pp. 2887–2901, 2008.

[43] C. Bellardita and O. Kiehn, "Phenotypic characterization of speed-associated gait changes in mice reveals modular organization of locomotor networks," *Current Biology*, vol. 25, no. 11, pp. 1426–1436, 2015.

[44] L. E. Spardy, S. N. Markin, N. A. Shevtsova, B. I. Prilutsky, I. A. Rybak, and J. E. Rubin, "A dynamical systems analysis of afferent control in a neuromechanical model of locomotion: Ii. phase asymmetry," *Journal of neural engineering*, vol. 8, no. 6, p. 065004, 2011.

[45] I. A. Rybak, N. A. Shevtsova, M. Lafreniere-Roula, and D. A. McCrea, "Modelling spinal circuitry involved in locomotor pattern generation: insights from deletions during fictive locomotion," *The Journal of physiology*, vol. 577, no. 2, pp. 617–639, 2006.

[46] D. A. McCrea and I. A. Rybak, "Organization of mammalian locomotor rhythm and pattern generation," *Brain research reviews*, vol. 57, no. 1, pp. 134–146, 2008.

[47] M. D. McDonnell, K. Boahen, A. Ijspeert, and T. J. e. Sejnowski, "Engineering intelligent electronic systems based on computational neuroscience," *Proceedings of the IEEE*, vol. 102, no. 5, pp. 646–651, 2014.

[48] A. Espinal, H. Rostro-Gonzalez, M. Carpio, E. I. Guerra-Hernandez, M. Ornelas-Rodriguez, H. Puga-Soberanes, M. A. Sotelo-Figueroa, and P. Melin, "Quadrupedal robot locomotion: a biologically inspired approach and its hardware implementation," *Computational intelligence and neuroscience*, vol. 2016, 2016.

[49] S. Joucla, M. Ambroise, T. Levi, T. Lafon, P. Chauvet, S. Saïghi, Y. Bornat, N. Lewis, S. Renaud, and B. Yvert, "Generation of locomotor-like activity in the isolated rat spinal cord using intraspinal electrical microstimulation driven by a digital neuromorphic CPG," *Frontiers in neuroscience*, vol. 10, 2016.

Matteo Lodi was born in Genoa, Italy, in 1991. He received the "Laurea" (M.Sc.) five-year degree (Summa Cum Laude) in Electronic Engineering in 2015 and is currently working towards his Ph.D. degree in Electrical Engineering at the University of Genoa, Italy. He was a visitor to Georgia State University, Atlanta, USA, in 2016. His main research interests are in the area of modeling of nonlinear systems (hysteresis and networks of biological neurons), bifurcation analysis and nonlinear dynamics.

Andrey Shilnikov was born in Nizhny Novgorod, Russia, in 1962. He received M.S. in Mathematics & Physics in 1984, and Ph.D. in Differential Equations incl. Mathematical Physics, in 1990 both from University of Nizhny Novgorod, Russia. He was a postdoctoral fellow at UC Berkeley in 1993-1994, 1995-1996, and a Royal Society Postdoctoral Fellow at Cambridge University, UK in 1994-1995. Prior to joining GSU in 2000, he held visiting positions at UC Berkeley, Georgia Institute of Technology, and Cornell University. Dr. Shilnikov is Professor of Applied Mathematics and Mathematical Neuroscinece with a joint appointment at Neuroscience Institute and Department of Mathematics & Statistics at GSU. He is a faculty of Center for Nonlinear Science at Georgia Institute of Technology, and a member of GSU Center for Behavioral Neuroscience. His original area of expertise is the theory of applied dynamical systems and global bifurcations. He studies dynamics and their origin in diversely phenomenological systems and in exact models from life sciences. Of his special interest is a new emergent crossdisciplinary field known as mathematical neuroscience. Its scopes include nonlinear models of individual neurons and networks. His lab develops advanced mathematical tools paired with sophisticated computations. He is an author of about 100 scholarly publications, including several advanced textbooks on dynamical systems. He presented many plenary and invited talks at various meetings and colloquium talks at national universities and around the globe, and co-organized more than 30 conferences, workshops and special sessions nation- and worldwide. Dr. Shilnikov currently serves on Editorial board of J. Mathematical Neuroscience J. Frontiers of Applied Mathematics and J. Discontinuity, Nonlinearity & Complexity.

Marco Storace (M'01, SM'14) was born in Genoa, Italy, in 1969. He received the "Laurea" (M.Sc.) five-year degree (Summa Cum Laude) in Electronic Engineering in March 1994 and the Ph.D. degree in Electrical Engineering in April 1998, both from the University of Genoa, Italy. Since 2011 he has been a Full Professor in the University of Genoa, now in the Department of Electrical, Electronic, Telecommunications Engineering and Naval Architecture. He was a visitor to EPFL, Lausanne, Switzerland, in 1998 and 2002. His main research interests are in the area of nonlinear circuit theory and applications, with emphasis on (circuit) models of nonlinear systems (e.g., hysteresis, biological neurons), methods for the piecewise-linear approximation of nonlinear systems and for the consequent circuit synthesis, bifurcation analysis and nonlinear dynamics. He is the author or coauthor of more than 130 scientific papers, more than an half of which have been published in international journals. He served as Associate Editor of the IEEE TRANSACTIONS ON CIRCUITS AND SYSTEMS – II (2008-2009) and is member of the IEEE Technical Committee on Nonlinear Circuits and Systems (TC-NCAS).